

## Supporting Information

### Metallo-supramolecular polymers engineered porous carbon frameworks encapsulated stable ultra-small nanoparticles: a general approach to construct highly dispersed catalysts

Yongjian Ai,<sup>a</sup> Mengqi He,<sup>b</sup> Feng Zhang,<sup>a</sup> Yang Long,<sup>a</sup> Yunzheng Li,<sup>a</sup> Qiang Han,<sup>a</sup> Mingyu Ding,<sup>a</sup> Hong-bin Sun,\*<sup>b</sup> and Qionglin Liang\*<sup>a</sup>

<sup>a</sup>*Key Laboratory of Bioorganic Phosphorus Chemistry & Chemical Biology (Ministry of Education), Beijing Key Lab of Microanalytical Methods & Instrumentation, Department of Chemistry, Tsinghua University, Beijing 100084, P.R. China*

<sup>b</sup>*Department of Chemistry, Northeastern University, Shenyang 110819, P.R. China*

\* liangql@tsinghua.edu.cn

\* sunhb@mail.neu.edu.cn

#### Table of contents

1. General information of characterization.....	S2
2. Materials characterization.....	S3-S8
3. Comparison of catalyst activity.....	S9
4. GC-MS data of Anilines.....	S9-S12
References.....	S13-S14

## **1. General information of characterization**

The materials morphology was observed by the JEOL SU-8010 scanning electron microscopy (SEM) and JEM-2100F high resolution transmission electron microscopy (HR-TEM). The scanning transmission electron microscopy (STEM) and energy-dispersive X-ray spectroscopy (EDS) are accessories of the HR-TEM apparatus. Fourier transform infrared (FT-IR) spectra were obtained by a Bruker IFS28 spectrometer in the region of 4000–500 cm<sup>-1</sup>. The solid-state nuclear magnetic resonance (NMR) instrument was JEOL JNMECZ600R. The X-ray diffraction (XRD) experiments were recorded on a Rigaku corporation Smart-Lab, diffractometer using Cu K $\alpha$  radiation ( $\lambda = 0.1541$  nm). X-ray photoelectron spectroscopy (XPS) measurements were performed using a PHI Quantera SXM spectrometer, ULVAC-PHI, and the binding energy determination was based on the C 1s at 284.8 eV with an experimental error of  $\pm 0.2$  eV. Nitrogen adsorption/desorption measurements were conducted with a Tristar II 3020 volumetric adsorption analyzer at -196 °C. Thermogravimetric analysis (TGA) was carried with a STA449F3 instrument under air atmosphere. Raman spectra were recorded with a Horiba HR-800 spectrometer equipped with a charge coupled device detector cooled by liquid nitrogen. The inductively coupled plasma mass spectrometry (ICP-MS) is PerkinElmer ELAN DRC-e. The AFM was Cypher S (Asylum Research). The detailed reaction procedure was further detected by the UV-visible spectrophotometer (UV-6100 double-beam spectrophotometer). This reaction system was also applied to the hydrogenation of varieties of nitroaromatics with different functional groups. All reactions were monitored by TLC (petroleum ether/ethyl acetate), HPLC (Waters, Kromasil 5mm C18 column) and detected by GC-MS (Bruker 450GC-320MS).

## 2. Materials characterization

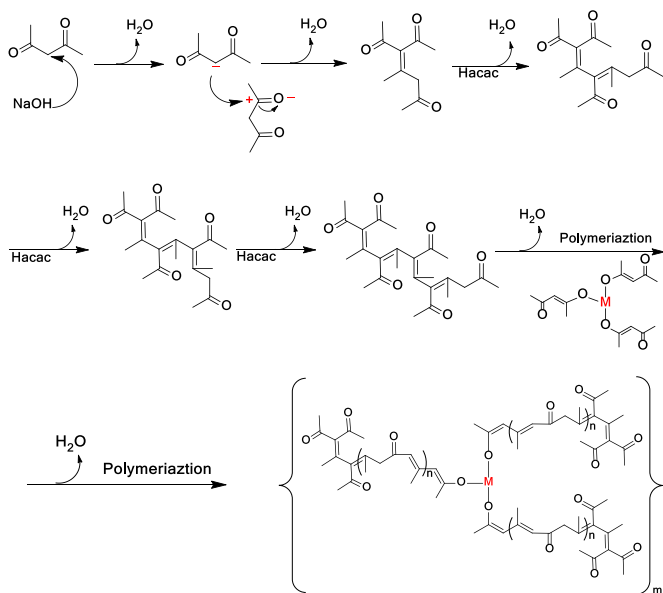


**Figure S1.** Pathway for the fabrication of metallo-supramolecular polymers.

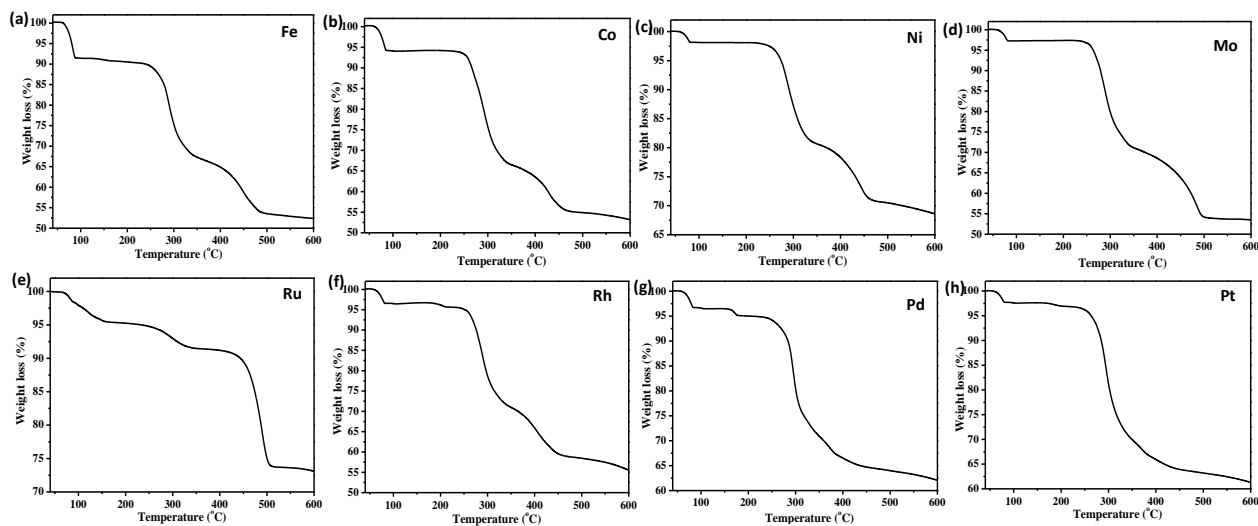


**Figure S2.** TGA curves of the metallo-supramolecular polymer precursor: (a) Fe, (b) Co, (c) Ni, (d) Mo, (e) Ru, (f) Rh, (g) Pd, (h) Pt.

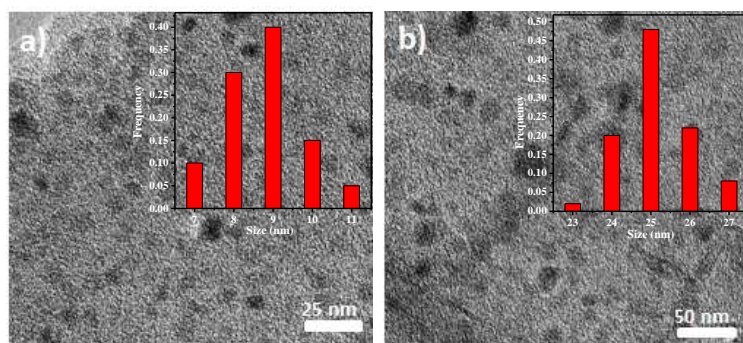


**Figure S3.** HR-TEM images of Pd@PCF that the polymer precursors annealed at (a) 600 °C and (b) 800 °C.

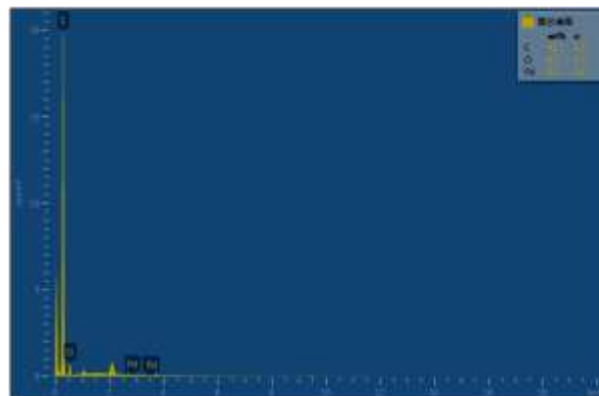


**Figure S4.** EDS spectrum of Pd@PCF.

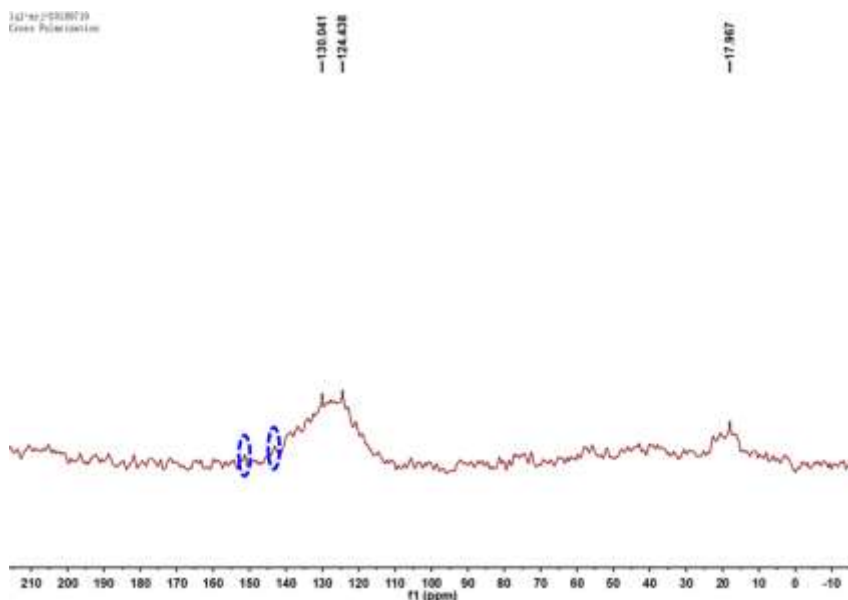


**Figure S5.** (a) The solid-state  $^{13}\text{C}$  NMR of Pd@PCF.

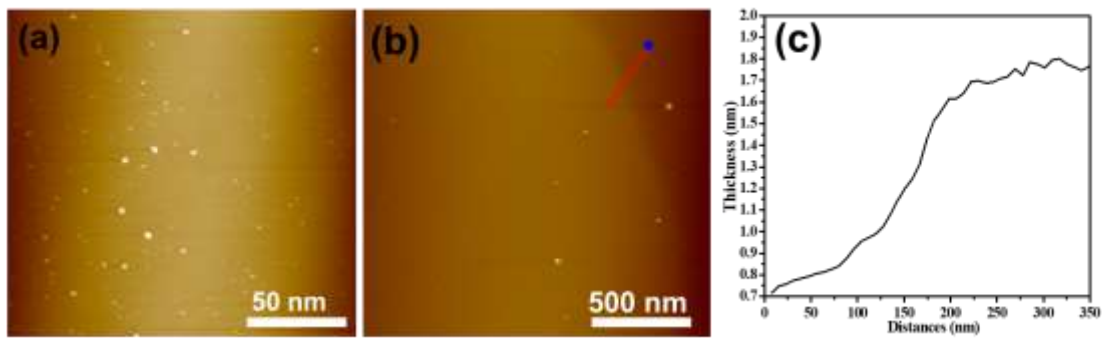


**Figure S6.** (a) AFM images of the Pd@PCF nanocatalysts, (b-c) the thickness of the PCF.

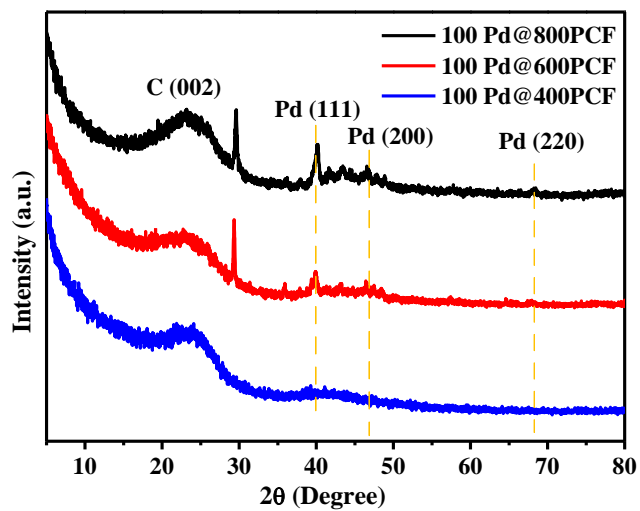


**Figure S7.** The XRD pattern of Pd@PCF annealed at different temperature.

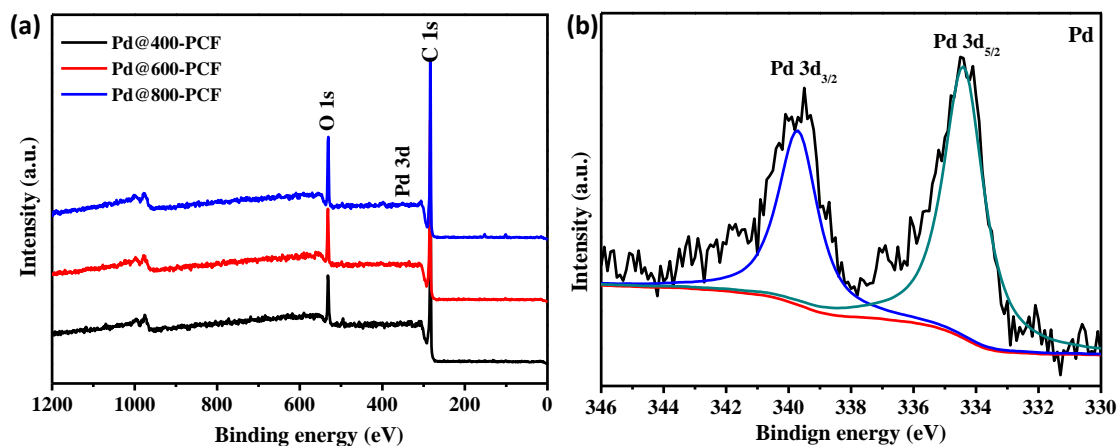


**Figure S8.** (a) XPS survey spectrum of the Pd@PCF obtained from different temperature; (b) XPS spectrum of the Pd 3d region of Pd@PCF.

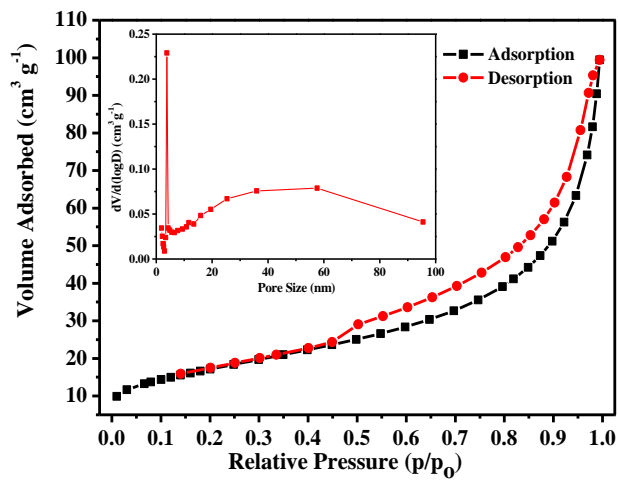


**Figure S9.** Nitrogen adsorption/desorption isotherms of the Pd@PCF nanocatalysts.

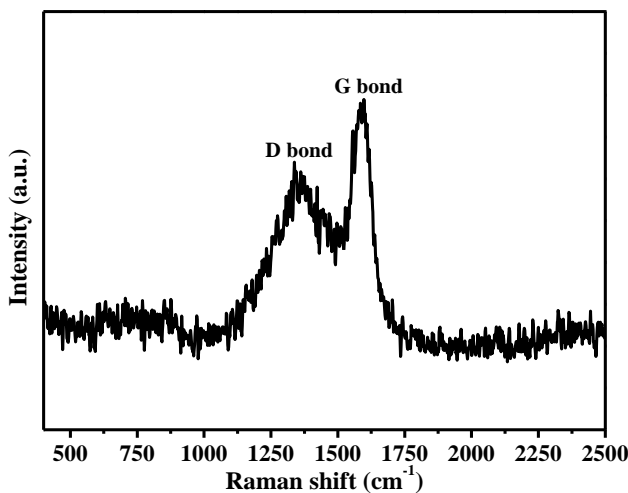


**Figure S10.** Raman spectra of the Pd@PCF nanocatalysts.

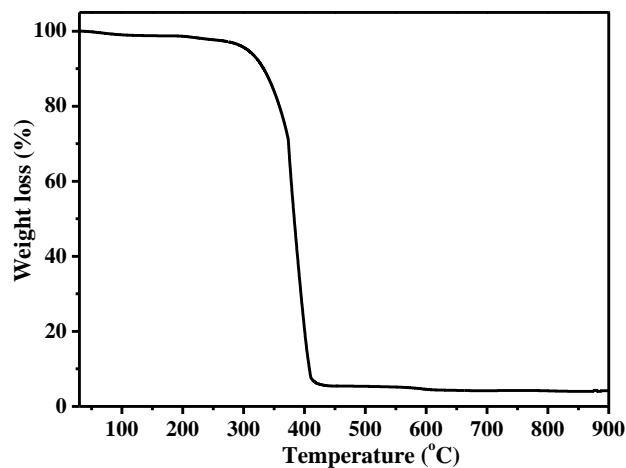


**Figure S11.** TGA curves of the Pd@PCF nanocatalysts (air atmosphere).

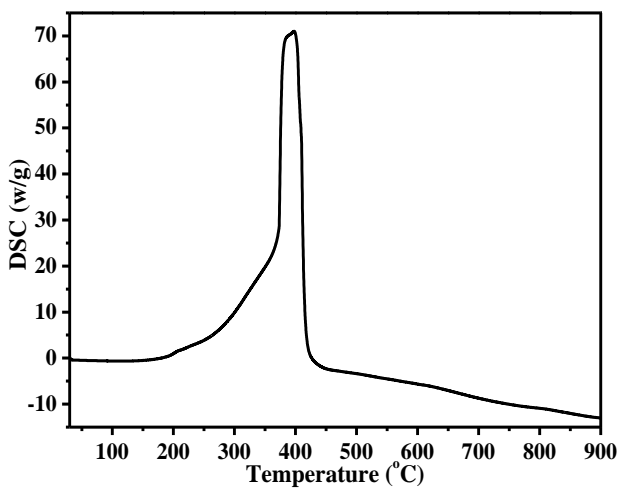


**Figure S12.** DSC curves of the Pd@PCF nanocatalysts (air atmosphere)

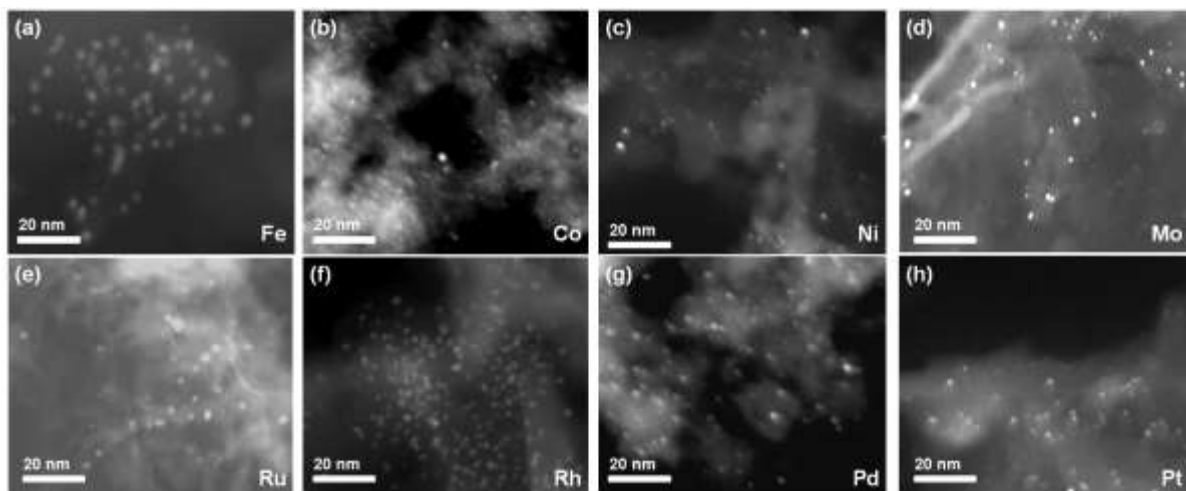


**Figure S13.** STEM images of M@PCF: (a) Fe, (b) Co, (c) Ni, (d) Mo, (e) Ru, (f) Rh, (g) Pd, (h) Pt

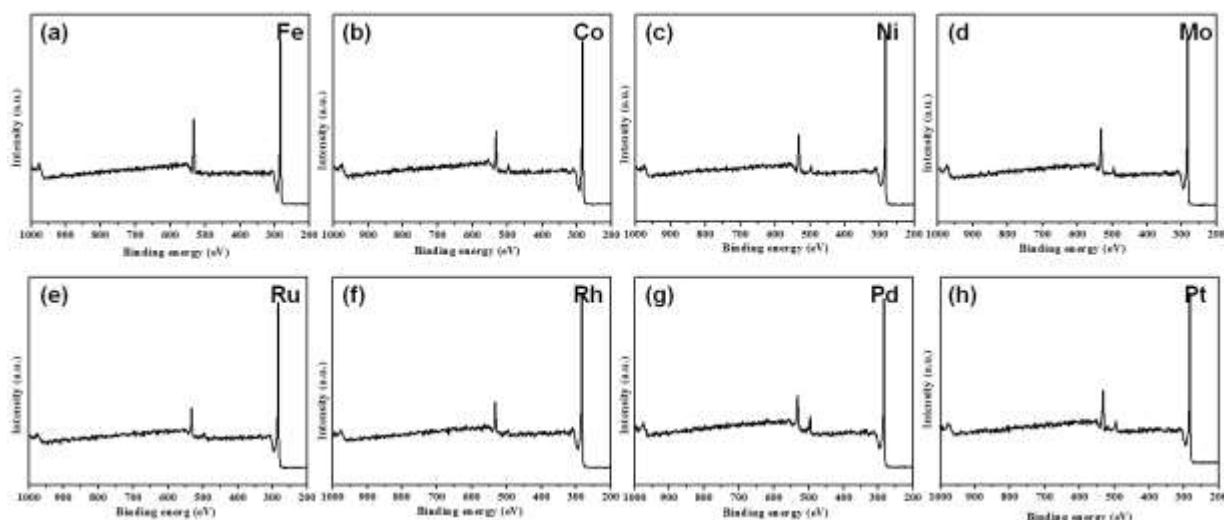


**Figure S14.** XPS survey spectroscopy of M@PCF: (a) Fe, (b) Co, (c) Ni, (d) Mo, (e) Ru, (f) Rh, (g) Pd, (h) Pt



**Figure S15.** TEM image of ultra-small Pd nanoparticles as Prasad reported.

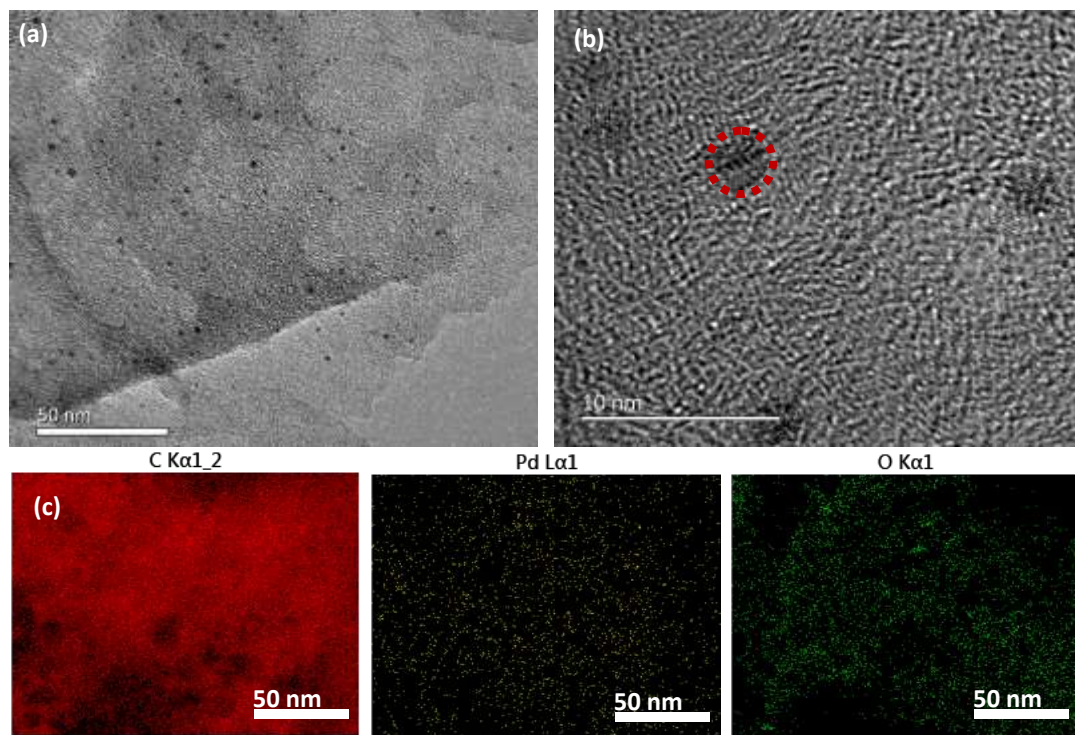


**Figure S16.** (a-b) HRTEM, (c) EDS images of Pd@PCF after used for 10 cycles.

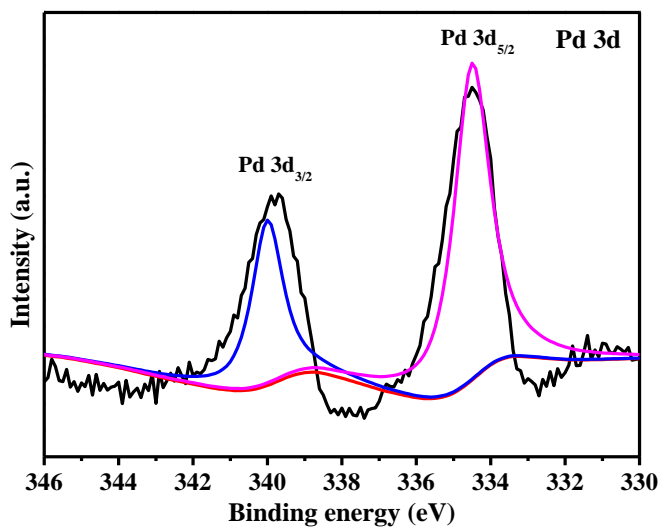


Figure S17. XPS spectrum of the Pd 3d region of the reused Pd@PCF.

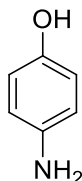
### 3. Comparison of catalyst activity

**Table S1.** Comparison of the ability of various noble metal-based catalysts for catalyzing hydrogenation of nitroarenes.

Entry	Catalyst	Reactant	Time (min)	Conv. (%)	TOF ( $\text{h}^{-1}$ )	Ref.
1	Pd NP/CNT	4-nitrophenol	7	>99	1080	1
2	Pd@CPP-F	nitrobenzene	60	>99	228	2
3	PdsNC/PN-CeO <sub>2</sub>	4-nitrophenol	120	>99	10900	3
4	Pd/CNT <sub>EG</sub>	4-chloronitrobenzene	120	>99	7440	4
5	Pd@Beta	4-chloronitrobenzene	120	>99	1520	5
6	Pd/Gd(OH) <sub>3</sub>	4-nitrophenol	1	>99	2176	6
7	Pd/MCB-EG	nitrate	150	>99	366	7
8	GO@AC/Pd	4-nitrophenol	1.65	>99	36120	8
9	Pd/TiO <sub>2</sub>	4-nitrophenol	5	90	560	9
10	Pt/FeOx	3-nitrostyrene	50	>99	1500	10
11	PtNPs@COF	4-nitrophenol	8	>99	17	11
12	RhNPs/SBA-NH <sub>2</sub>	4-nitrophenol	10	>99	3059	12
13	RhNPs	4-nitrophenol	7	>99	4373	13
14	Ru/CNTs-ht	4-chloronitrobenzene	240	>99	694	14
15	Ru Complex	4-nitrophenol	1200	>99	0.5	15
16	Fe <sub>3</sub> O <sub>4</sub> /C@Au	4-nitrophenol	3.3	>99	1044	16
17	Au/NPG	3-nitrostyrene	720	85	0.35	117
18	AgNCs	4-nitrophenol	120	>99	67	18
19	Pd@PCF-400	4-nitrophenol	4	>99	11400	This work

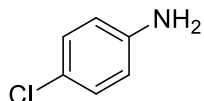
#### 4. GC-MS Data of Anilines:

##### 4-Aminophenol (Table 2, entry 1):



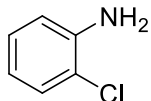
GC-MS:  $m/z$  (%) 109 (100)  $[M]^+$ , 80 (50), 52 (14).<sup>[19]</sup>

##### 4-Chlorobenzenamine (Table 2, entry 2):



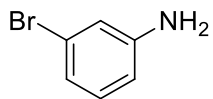
GC-MS:  $m/z$  (%) 127 (100)  $[M]^+$ , 92 (13), 65 (21).<sup>[20]</sup>

##### 2-Chloroaniline (Table 2, entry 3):



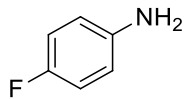
GC-MS:  $m/z$  (%) 127 (100)  $[M]^+$ , 92 (14), 65 (17).<sup>[21]</sup>

##### 3-Bromoanilines (Table 2, entry 4)



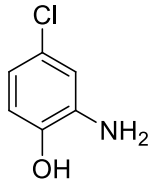
GC-MS:  $m/z$  (%) 173 (100)  $[M]^+$ , 92 (91), 65 (85).<sup>[21]</sup>

##### 4-Fluoroaniline (Table 2, entry 5)



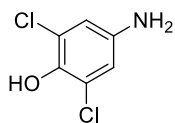
GC-MS:  $m/z$  (%) 111 (100)  $[M]^+$ , 84 (43), 57 (11).<sup>[21]</sup>

##### 2-Hydroxy-5-chloro-aniline (Table 2, entry 6):



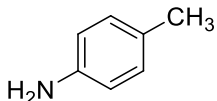
GC-MS:  $m/z$  (%) 143 (100)  $[M]^+$ , 114 (14), 80 (31), 51 (10).<sup>[22]</sup>

##### 2,6-Dichloro-4-aminophenol (Table 2, entry 7):



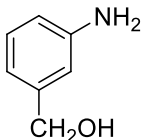
GC-MS: m/z (%) 177 (100) [M]<sup>+</sup>, 113 (87), 78 (60), 52 (16).<sup>[22]</sup>

**4-Toluidine (Table 2, entry 8):**



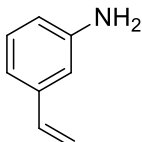
GC-MS: m/z (%) 106 (100) [M]<sup>+</sup>, 77 (12). Physical and spectral data were consistent with those previously reported.<sup>[23]</sup>

**(3-Aminophenyl)-methanol (Table 2, entry 9):**



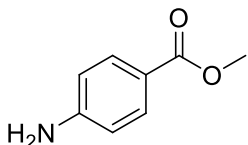
GC-MS: m/z (%) 123 (100) [M]<sup>+</sup>, 94 (74), 77 (30), 65 (13), 39 (8).<sup>[24]</sup>

**3-Aminostyrene (Table 2, entry 10):**



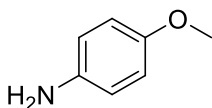
GC-MS: m/z (%) 119 (100) [M]<sup>+</sup>, 91 (28), 89 (5), 65 (13).<sup>[25]</sup>

**Methyl 4-aminobenzoate (Table 2, entry 11):**



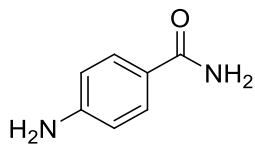
GC-MS: m/z (%) 151 (54) [M]<sup>+</sup>, 120 (100), 92 (26), 65 (20).<sup>[26]</sup>

**4-Methoxyaniline (Table 2, entry 12):**



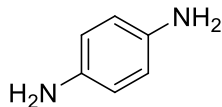
GC-MS: m/z (%) 108 (100) [M]<sup>+</sup>, 80 (36), 53 (14).<sup>[26]</sup>

**4-Aminobenzamide (Table 2, entry 13):**



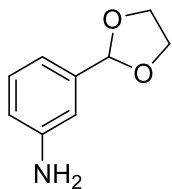
GC-MS:  $m/z$  (%) 136 (73) [M]<sup>+</sup>, 120 (100), 92 (34), 65 (27), 39 (8).<sup>[23]</sup>

**1,4-Benzenediamine (Table 2, entry 14):**



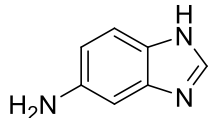
GC-MS:  $m/z$  (%) 108 (100) [M]<sup>+</sup>, 80 (33), 53 (10).<sup>[22]</sup>

**5-(Aminophenyl)-1,3-dioxolane (Table 2, entry 15):**



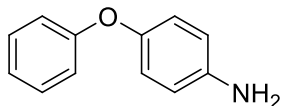
GC-MS:  $m/z$  (%) 165 (99) [M]<sup>+</sup>, 120 (52), 93 (100), 65 (26).<sup>[23]</sup>

**6-Amino-1H-benzimidazole (Table 2, entry 16):**



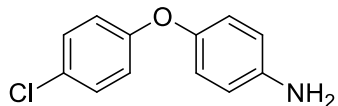
GC-MS:  $m/z$  (%) 133 (100) [M]<sup>+</sup>, 106 (15), 78 (8), 52 (12).<sup>[21]</sup>

**4-Aminodiphenyl ether (Table 2, entry 17):**



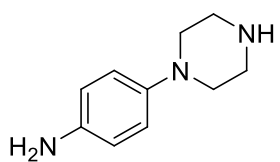
GC-MS:  $m/z$  (%) 185 (100) [M]<sup>+</sup>, 156 (17), 108 (74), 80 (25), 51 (13).<sup>[27]</sup>

**4-(4-Chlorophenoxy)benzenamine (Table 2, entry 18):**



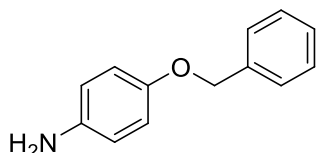
GC-MS:  $m/z$  (%) 219 (72) [M]<sup>+</sup>, 156 (13), 108 (100), 80 (30).<sup>[24]</sup>

**1-(4-Aminophenyl)piperazine (Table 2, entry 19):**



GC-MS:  $m/z$  (%) 177 (51) [M]<sup>+</sup>, 135 (100), 120 (30), 92 (10) 65 (11).<sup>[27]</sup>

#### 4-(Benzylamino)benzenamine (Table 2, entry 20):



GC-MS:  $m/z$  (%) 199 (15) [M]<sup>+</sup>, 108 (100), 91 (29), 80 (14), 53 (5).<sup>[28]</sup>

#### References

- [1]. Gu, X.; Qi, W.; Xu, X.; Sun, Z.; Zhang, L.; Liu, W.; Pan, X.; Su. D. S. Covalently functionalized carbon nanotube supported Pd nanoparticles for catalytic reduction of 4-nitrophenol. *Nanoscale* **2014**, *6*, 6609–6616.
- [2]. Li, L.; Zhou, C.; Zhao, H.; Wang, R. Spatial control of palladium nanoparticles in flexible click-based porous organic polymers for hydrogenation of olefins and nitrobenzene. *Nano Res.* **2015**, *8*, 709–721.
- [3]. Zhang, S.; Chang, C. R.; Huang, Z. Q.; Li, J.; Wu, Z. M.; Ma, Y. Y.; Zhang, Z. Y.; Wang, Y.; Qu, Y. Q. High catalytic activity and chemoselectivity of sub-nanometric Pd clusters on porous nanorods of CeO<sub>2</sub> for hydrogenation of nitroarenes. *J. Am. Chem. Soc.* **2016**, *138*, 2629–2637.
- [4]. Dongil, A. B.; Pastor-Pérez, L.; Fierro, J. L. G.; Escalona, N.; Sepúlveda-Escribano, A. Synthesis of palladium nanoparticles over graphite oxide and carbon nanotubes by reduction in ethylene glycol and their catalytic performance on the chemoselective hydrogenation of para-chloronitrobenzene. *Appl. Catal. A: Gen.* **2016**, *513*, 89–97.
- [5]. Zhang, J.; Wang, L.; Shao, Y.; Wang, Y. Q.; Gates, B. C.; Xiao, F. S. A Pd@Zeolite catalyst for nitroarene hydrogenation with high product selectivity by sterically controlled adsorption in the zeolite micropores. *Angew. Chem. Int. Ed.* **2017**, *56*, 9747–9751.
- [6]. Ullah, N.; Imran, M.; Liang, K.; Yuan, C. Z.; Zeb, A.; Jiang, N.; Qazi, U. Y.; Sahar, S.; Xu, A. W. Highly dispersed ultra-small Pd nanoparticles on gadolinium hydroxide nanorods for efficient hydrogenation reactions. *Nanoscale* **2017**, *9*, 13800–13807.
- [7]. Ye, T.; Durkin, D. P.; Banek, N. A.; Wagner, M. J.; Shuai, D. M. Graphitic carbon nitride supported ultrafine Pd and Pd–Cu catalysts: enhanced reactivity, selectivity, and longevity for nitrite and nitrate hydrogenation *ACS Appl. Mater. Interfaces*. **2017**, *9*, 27421–27126.
- [8]. Xi, J. B.; Sun, H. Y.; Wang, D.; Zhang, Z. Y.; Duan, X. M.; Xiao, J. W.; Xiao, F.; Liu, S. L. M.; Wang, S. Confined-interface-directed synthesis of Palladium single-atom catalysts on graphene/amorphous carbon. *Appl. Catal. B: Environ.* **2018**, *225*, 291–297.
- [9]. Rogers, S. M.; Catlow, C. R. A.; Gianolio, D.; Wells, P. P.; Dimitratos, N. Supported metal nanoparticles with tailored catalytic properties through sol-immobilisation: applications for the hydrogenation of nitrophenols.

*Faraday Discuss.* **2018**, DOI: 10.1039/c7fd00216e.

- [10]. Wei, H. S.; Liu, X. Y.; Wang, A. Q.; Zhang, L. L.; Qiao, B. T.; Yang, X. F.; Huang, Y. Q.; Miao, S.; Liu, J. Y.; Zhang, T. FeOx-supported platinum single-atom and pseudo-single-atom catalysts for chemoselective hydrogenation of functionalized nitroarenes. *Nat. Commun.* **2014**, *5*, 5634–5642.
- [11]. Lu, S. L.; Hu, Y. M.; Wan, S.; McCaffrey, R.; Jin, Y. H.; Gu, H. W.; Zhang, W. Synthesis of ultrafine and highly dispersed metal nanoparticles confined in a thioether-containing covalent organic framework and their catalytic applications. *J. Am. Chem. Soc.* **2017**, *139*, 17082–17088.
- [12]. Ganji, S.; Enumula, S. S.; Marella, R. K.; Rao, K. S. R.; Burri, D. R. RhNPs/SBA-NH<sub>2</sub>: a high-performance catalyst for aqueous phase reduction of nitroarenes to aminoarenes at room temperature. *Catal. Sci. Technol.* **2014**, *4*, 1813–1819.
- [13]. Zhou, J. J.; Li, Y. N.; Sun, H. B.; Tang, Z. K.; Qi, L.; Liu, L.; Ai, Y. Y.; Li, S.; Shao, Z. X.; Liang, Q. L. Porous silica-encapsulated and magnetically recoverable Rh NPs: a highly efficient, stable and green catalyst for catalytic transfer hydrogenation with “slow-release” of stoichiometric hydrazine in water. *Green. Chem.* **2017**, *19*, 3400–3407.
- [14]. Wang, Y.; Rong, Z.; Wang, Y.; Zhang, P.; Wang, Y.; Qu, J. Ruthenium nanoparticles loaded on multiwalled carbon nanotubes for liquid-phase hydrogenation of fine chemicals: An exploration of confinement effect. *J. Catal.* **2015**, *329* 95–106.
- [15]. Wei, Jia, H. Zhang, T. i Zhang, D. Xie, S. Ling, E. Sheng, Half-sandwich ruthenium complexes with schiff-base ligands: syntheses, characterization, and catalytic activities for the reduction of nitroarenes. *Organometallics.* **2016**, *35*, 503–512.
- [16]. Zeng, T.; Zhang, X. Wang, S. Ma, Y.; Niu, H.; Cai, Y. A double-shelled yolk-like structure as an ideal magnetic support of tiny gold nanoparticles for nitrophenol reduction. *J. Mater. Chem. A.* **2013**, *1*, 11641–11647.
- [17]. Guo, H.; Yan, X.; Zhi, Y.; Li, Z.; Wu, C.; Zhao, C.; Wang, J.; Yu, Z.; Ding, Y.; He, W.; Li, Y. D. Nanostructuring gold wires as highly durable nanocatalysts for selective reduction of nitro compounds and azides with organosilanes. *Nano Res.* **2015**, *8*, 1365–1372.
- [18]. Giri, S.; Das, R.; Westhuyzen, C.; Maity, A. An efficient selective reduction of nitroarenes catalyzed by reusable silver-adsorbed waste nanocomposite. *Appl. Cata. B: Environ.* **2017**, *209*, 669–678.
- [19] Feng, W.; Dong, H.; Niu, L.; Wen, X.; Huo, L.; Bai, G. A novel Fe<sub>3</sub>O<sub>4</sub>@nSiO<sub>2</sub>@NiPd-PVP@mSiO<sub>2</sub> multi-shell core-shell nanocomposite for cinnamic acid hydrogenation in water. *J. Mater. Chem. A.* **2015**, *3*, 19807–19814.
- [20] Beswick, O.; Yuranov, I.; Alexander, D. T. L.; Kiwi-Minsker, L. Iron oxide nanoparticles supported on activated carbon fibers catalyze chemoselective reduction of nitroarenes under mild conditions. *Catal. Today.* **2015**, *249*, 45–51.
- [21] Rahaim, R. J.; Maleczka, R. E. Pd-catalyzed silicon hydride reductions of aromatic and aliphatic nitro groups. *Org. Lett.* **2005**, *7*, 5087–5090.
- [22] AIST: Integrated Spectral Database System of Organic Compounds. (Data were obtained from the National Institute of Advanced Industrial Science and Technology (Japan))
- [23] Sun, S.; Quan, Z. J.; Wang, X. C. Selective reduction of nitro-compounds to primary amines by nickel-catalyzed hydrosilylative reduction. *RSC Advance.* **2015**, *5*, 84574–84577.

- [24] Sharma, U.; Verma, P. K.; Kumar, N.; Kumar, V.; Bala, M.; Singh, B. Phosphane-free green protocol for selective nitro reduction with an iron-based catalyst. *Chem. Eur. J.* **2011**, 17, 5903.
- [25] Saha, A.; Ranu, B. Highly Chemoselective Reduction of Aromatic Nitro Compounds by Copper Nanoparticles/Ammonium Formate., *J. Org. Chem.* **2008**, 73, 6867.
- [26] Huang, X.; Buchwald, S. New ammonia equivalents for the Pd-catalyzed amination of aryl halides. *Org. Lett.* **2001**, 3, 3417–3419.
- [27] Maiti, D.; Buchwald, S. L. Orthogonal Cu-and Pd-based catalyst systems for the O-and N-arylation of aminophenols. *J. Am. Chem. Soc.* **2009**, 131, 17423–17429.
- [28] Yang, H.; Li, Y.; Jiang, M.; Wang, J.; Fu, H. General copper-catalyzed transformations of functional groups from arylboronic acids in water. *Chem. Eur. J.* **2011**, 17, 5652–5660.